SIAM J. SCI. COMPUT.
Vol. 32, No. 3, pp. 1346–1360

A POSTERIORI ERROR ESTIMATES OF STABILIZATION OF LOW-ORDER MIXED FINITE ELEMENTS FOR INCOMPRESSIBLE FLOW*

HAIBIAO ZHENG†, YANREN HOU‡, AND FENG SHI‡

Abstract. In this paper, we derive a posteriori error estimates for the stabilization of low-order mixed finite element methods for the Stokes equations. By defining different projection estimators, we prove that, up to higher order perturbation terms, the estimators yield global upper and lower bounds on the error of stabilized finite element methods. In numerical tests, each error estimator is shown to be equivalent to the discretization error. It is also shown that the adaptive strategy based on both projection estimators is efficient to detect local singularities in the flow problems.

Key words. Stokes equations, stabilized finite element methods, a posteriori error estimates, projection estimators

AMS subject classifications. 65M55, 65M70, 65N30, 65N50

DOI. 10.1137/090771508

1. Introduction.

The importance of a posteriori error estimates for controlling an automatic, self-adaptive mesh-refinement process is well established in recent decades; see Babuška and Rheinboldt [1, 2] and Verfurth [3] for a recent review. Many other researchers also pay attention to this field and have obtained many good results. For the literature, the readers are referred to recent works [4, 5, 6, 7, 8, 9, 10, 11, 12, 13, 14, 15, 16, 17].

Deriving a posteriori error estimates for the Stokes equations also has received much attention. The work of Verfurth [14] and Bank and Welfert [15] builds the basic foundation for the mathematical analysis of practical methods and has been advanced by Ainsworth and Oden [16] and others. The compatibility of velocity and pressure achieved by satisfying the discrete inf-sup condition is a key factor for solving the impressible flow problems. Thus, there are many stabilized finite element methods to circumvent the inf-sup condition, such as the mini-element method and the pressure projection stabilized finite element methods; see [18, 19, 20, 21, 22]. Based on the attractive features of the adaptive methods and stabilized methods, recently some scholars have tried to combine them [17].

In this paper, based on the work of Bochev, Dohrmann, and Gunzburger [21], we propose two new projection estimators and derive a posteriori error estimates for the stabilization of mixed low-order finite elements of the Stokes equations. The natural combination of adaptive techniques with stabilized methods retains the best features of both methods and overcomes many of their defects. Their implementation relies on the projection operators, whose actions use only standard nodal data structures and can be evaluated locally at the element level. Additionally, the combination turns out to be particularly attractive on modern parallel processing architectures. Finally, by

*Received by the editors September 17, 2009; accepted for publication (in revised form) February 25, 2010; published electronically May 14, 2010. This work was supported by the NSF of China (grant 10871156) and XJTU (grant 2009xjtujc30).

http://www.siam.org/journals/sisc/32-3/77150.html

†Corresponding author. College of Science, Xi'an Jiaotong University, Xi'an 710049, China (hbzheng13@gmail.com).

‡College of Science, Xi'an Jiaotong University, Xi'an 710049, China (yrhou@mail.xjtu.edu.cn, fengshi81@yahoo.com.cn).

assuming the nondegeneracy property, we can obtain global lower and upper bounds for the error of the numerical solution. Throughout this work, for simplicity we restrict our attention to triangular elements, and the extension to three-dimensional problems is straightforward.

The outline of the paper is as follows. Section 2 introduces the governing equations, the notation used throughout the paper, and some well-known results of the stabilized mixed low-order finite element methods. The projection error estimators are designed, and a posteriori error estimates are presented in section 3. Section 4 is a succinct summary of some implementation details, while some numerical simulations are presented in section 5 to illustrate the efficiency of the error estimators. We finish with a short conclusion in section 6.

2. Stabilization of low-order mixed finite elements for the Stokes equations. We consider the incompressible Stokes equations

$$\begin{aligned} -\Delta \mathbf{u} + \nabla p &= \mathbf{f} \quad \text{in } \Omega, \\ \nabla \cdot \mathbf{u} &= 0 \quad \text{in } \Omega, \\ \mathbf{u} &= 0 \quad \text{on } \partial\Omega, \end{aligned} \tag{2.1}$$

where Ω represents a polyhedral domain in $R^d, d = 2, 3$, with boundary $\partial\Omega$, $\mathbf{u}$ is the velocity vector, p is the pressure, and $\mathbf{f}$ is the prescribed body force.

The standard variational formulation of (2.1) is given by the following: find $(\mathbf{u}, p) \in (\mathbf{V}, S)$ satisfying

$$Q(\mathbf{u}, p; \mathbf{v}, q) = (\mathbf{f}, \mathbf{v}) \quad \forall (\mathbf{v}, q) \in (\mathbf{V}, S), \tag{2.2}$$

where

$$\mathbf{V} = \mathbf{H}_0^1(\Omega) \text{ and } S = L_0^2(\Omega) = \left\{ q \in L^2(\Omega); \int_\Omega q \mathbf{dx} = 0 \right\},$$

and

$$Q(\mathbf{u}, p; \mathbf{v}, q) = (\nabla \mathbf{u}, \nabla \mathbf{v}) - (\nabla \cdot \mathbf{v}, p) - (\nabla \cdot \mathbf{u}, q),$$

with $(\cdot, \cdot)$ the inner product in $L^2(\Omega)$ or in its vector value version. The norm and seminorm in $H^k(\Omega)^d$ are denoted by $|| \cdot ||_k$ and $| \cdot |_k$, respectively. The space $\mathbf{V}$ is equipped with the norm $\|\nabla \cdot\|_0$ or its equivalent norm $\|\cdot\|_1$ due to Poincare's inequality. Spaces consisting of vector-valued functions are denoted in boldface. Throughout the paper we use C to denote a generic positive constant whose value may change from place to place but remains independent of the mesh parameter h.

It is well known [23, 24] that $Q(\mathbf{u}, p; \mathbf{v}, q)$ satisfies the following inf-sup condition with a positive constant β_1:

$$\sup_{(\mathbf{v},q)\in(\mathbf{V},S)} \frac{Q(\mathbf{u}, p; \mathbf{v}, q)}{||\mathbf{v}||_1 + ||q||_0} \geq \beta_1 (||\mathbf{u}||_1 + ||p||_0) \quad \forall (\mathbf{u}, p) \in (\mathbf{V}, S), \tag{2.3}$$

which implies that problem (2.2) has a unique solution.

In this paper, we formulate the finite element methods for the Stokes equations based on a regular triangulation τ_h of the domain Ω with the mesh parameter $h = \max_{T\in\tau_h} diam(T)$. The set of all interior faces is denoted by Γ_h. The norm

$$||u||_{\Gamma_h} = \left(\sum_{E\in\Gamma_h} \int_E u^2 \mathbf{d}S \right)^{1/2}$$

will be useful in what follows.

Since our main focus is on low-order velocity and pressure pairs, we consider only the following finite element families:

$$R_1 = \{q_h \in C(\Omega) \mid q_h|_T \in P_1(T)\ \forall T \in \tau_h\},$$
$$R_0 = \{q_h \in L^2(\Omega) \mid q_h|_T \in P_0(T)\ \forall T \in \tau_h\},$$

where $P_1(T)$ is the space of linear polynomials on T and P_0 is a constant polynomial space on T.

In this paper, we will consider the lowest equal order C^0 velocity and pressure pair

$$\mathbf{V}^h = \mathbf{R}_1 \bigcap \mathbf{H}_0^1(\Omega) \text{ and } S^h = R_1 \bigcap L_0^2(\Omega), \tag{2.4}$$

and the lowest order conforming pair

$$\mathbf{V}^h = \mathbf{R}_1 \bigcap \mathbf{H}_0^1(\Omega) \text{ and } S^h = R_0 \bigcap L_0^2(\Omega). \tag{2.5}$$

As we know, both finite element pairs do not satisfy the discrete inf-sup condition.

Now, we recall the stabilized low-order mixed finite element methods for the Stokes equations in [21]: find $(\mathbf{u}^h, p^h) \in (\mathbf{V}^h, S^h)$ such that

$$\tilde{Q}(\mathbf{u}^h, p^h; \mathbf{v}^h, q^h) = (\mathbf{f}, \mathbf{v}^h) \quad \forall (\mathbf{v}^h, q^h) \in (\mathbf{V}^h, S^h). \tag{2.6}$$

Here

$$\tilde{Q}(\mathbf{u}^h, p^h; \mathbf{v}^h, q^h) = (\nabla \mathbf{u}^h, \nabla \mathbf{v}^h) - (\nabla \cdot \mathbf{v}^h, p^h) - (\nabla \cdot \mathbf{u}^h, q^h) - G(p^h, q^h)$$

and

$$G(p^h, q^h) = ((I - \Pi)p^h, (I - \Pi)q^h).$$

The projection operator Π is defined as follows:

$$\Pi = \begin{cases} \Pi_0 & \text{if } S^h \text{ is defined by (2.4)}, \\ \Pi_1 & \text{if } S^h \text{ is defined by (2.5)} \end{cases} \tag{2.7}$$

and

$$\Pi_0 : L^2(\Omega) \to R_0 \text{ and } \Pi_1 : L^2(\Omega) \to R_1. \tag{2.8}$$

In the following discussion, operator $\Pi^{d\times d}$, which acts on the velocity deformation tensor, is also denoted by Π for simplicity.

Remark 1. In fact, formulation (2.6) can be rewritten as

$$\begin{array}{ll} (\nabla \mathbf{u}^h, \nabla \mathbf{v}^h) - (\nabla \cdot \mathbf{v}^h, p^h) = (\mathbf{f}, \mathbf{v}^h) & \forall \mathbf{v}^h \in \mathbf{V}^h, \\ (\nabla \cdot \mathbf{u}^h, q^h) + G(p^h, q^h) = 0 & \forall q^h \in S^h. \end{array} \tag{2.9}$$

The second equation implies that $||\nabla \cdot \mathbf{u}^h||_0 \le C||(I - \Pi)p^h||_0$.

Based on the discussion in [21], there exists a positive constant β_2, whose value is independent of h, such that the following weak inf-sup condition holds:

$$\sup_{(\mathbf{v}^h, q^h) \in (\mathbf{V}^h, S^h)} \frac{\tilde{Q}(\mathbf{u}^h, p^h; \mathbf{v}^h, q^h)}{||\mathbf{v}^h||_1 + ||q^h||_0} \ge \beta_2(||\mathbf{u}^h||_1 + ||p^h||_0) \quad \forall (\mathbf{u}^h, p^h) \in (\mathbf{V}^h, S^h). \tag{2.10}$$

Hence, problem (2.6) has a unique solution $(\mathbf{u}^h, p^h)$, and the error estimate

$$\|\nabla(\mathbf{u}-\mathbf{u}^h)\|_0 + \|p-q^h\|_0 \le Ch\{\|\mathbf{u}\|_2 + ||p||_1\} \tag{2.11}$$

holds provided $(\mathbf{u}, p) \in (\mathbf{H}^2(\Omega), H^1(\Omega))$.

To get our error estimators, first we assume that Π has the following properties:

$$||\Pi q||_0 \le C||q||_0 \quad \forall q \in L^2(\Omega) \tag{2.12}$$

and

$$||(I-\Pi)q||_0 \le Ch||q||_1 \quad \forall q \in H^1(\Omega). \tag{2.13}$$

In addition, under some mild assumptions on τ_h, the following inverse inequalities hold [25] (which will be used later):

$$||\nabla q^h||_0 \le C_I h^{-1}||q^h||_0, \quad q^h \in R_1 \tag{2.14}$$

and

$$||[q^h]||_{\Gamma_h} \le C_I h^{-1/2}||q^h||_0, \quad q^h \in R_0, \tag{2.15}$$

where $[q^h]$ denotes the jump of $q_h \in R_0$ along the interior face. The related vector-valued versions also hold. Moreover, we require that both $\mathbf{u}$, p and a sequence of meshes τ_h satisfy the following nondegeneracy property: there exists a positive constant C independent of h such that

$$\|\nabla(\mathbf{u}-\mathbf{u}^h)\|_0 + \|p-q^h\|_0 \ge Ch. \tag{2.16}$$

As argued in [26], this is not a very restrictive condition in practice.

3. The projection error estimators. For simplicity, we define

$$|||(\mathbf{e}^h, \varepsilon^h)||| := ||\nabla \mathbf{e}^h||_0 + ||\varepsilon^h||_0 \quad \text{and} \quad |||(\mathbf{e}^h, \varepsilon^h)|||_{0,T} := ||\nabla \mathbf{e}^h||_{0,T} + ||\varepsilon^h||_{0,T},$$

where $\mathbf{e}^h := \mathbf{u} - \mathbf{u}^h$, $\varepsilon^h := p - p^h$.

Now, based on the residual between the gradient of the finite element solution velocity component $\nabla \mathbf{u}^h$, pressure component p^h, and their projections $\Pi\nabla\mathbf{u}^h$, Πp^h, our projection estimator can be constructed locally as follows.

Case 1. If S^h is defined by (2.4), then

$${}^0\eta_{\Pi,T} := ||(I-\Pi_1)\nabla \mathbf{u}^h||_{0,T} + ||(I-\Pi_0)p^h||_{0,T}.$$

Case 2. If S^h is defined by (2.5), then

$${}^1\eta_{\Pi,T} := ||(I-\Pi_1)\nabla \mathbf{u}^h||_{0,T} + ||(I-\Pi_1)p^h||_{0,T}.$$

So the global estimators can be defined as

$$\eta_\Pi := \begin{cases} {}^0\eta_\Pi = \left\{ \displaystyle\sum_{T\in\tau_h} \left({}^0\eta_{\Pi,T}\right)^2 \right\}^{1/2} & \text{if } S^h \text{ is defined by (2.4)}, \\ {}^1\eta_\Pi = \left\{ \displaystyle\sum_{T\in\tau_h} \left({}^1\eta_{\Pi,T}\right)^2 \right\}^{1/2} & \text{if } S^h \text{ is defined by (2.5)}. \end{cases} \tag{3.1}$$

Remark 2. We should note that Π acting on the velocity deformation tensor is always chosen as Π_1, and Π acting on pressure will be determined according to (2.7).

Before giving the global upper and lower bounds, we recall a lemma presented in [21].

LEMMA 3.1. *There exists a positive constant C such that*

$$Ch||\nabla q^h||_0 \leq ||(I-\Pi_0)q^h||_0 \quad \forall q^h \in R_1, \tag{3.2}$$

$$Ch^{1/2}|||[q^h]|||_{\Gamma_h} \leq ||(I-\Pi_1)q^h||_0 \quad \forall q^h \in R_0. \tag{3.3}$$

Remark 3. Noting the velocity deformation tensor $\nabla \mathbf{u}^h \in R_0^{d\times d}$ and the proof in [21], the tensor-valued version of (3.3) also holds:

$$Ch^{1/2}|||[\nabla \mathbf{u}^h]|||_{\Gamma_h} \leq ||(I-\Pi_1)\nabla \mathbf{u}^h||_0 \quad \forall \mathbf{u}^h \in \mathbf{V}^h. \tag{3.4}$$

After the above preparations, we can derive a posteriori error estimates based on the projection estimators.

THEOREM 3.2. *There is a constant C which depends only on the smallest angle in the triangulation τ_h and the domain Ω such that, by assuming the nondegeneracy property of τ_h, the following global upper and lower bounds hold:*

$$\eta_\Pi \leq C|||(\mathbf{e}^h, \varepsilon^h)||| \tag{3.5}$$

and

$$|||(\mathbf{e}^h, \varepsilon^h)||| \leq C\left\{\eta_\Pi + h||\mathbf{f}-\mathbf{f}^h||_0\right\}. \tag{3.6}$$

Remark 4. Here, $\mathbf{f}^h \in \mathbf{V}^h$ is an arbitrary pointwise interpolation approximation of $\mathbf{f}$. The second term on the right-hand side of estimate (3.6) is of higher order perturbation.

Proof. Combining (2.11), (2.12), (2.13), and (2.16), we obtain that

$$\begin{aligned}
\eta_\Pi &= ||(I-\Pi_1)\nabla \mathbf{u}^h||_0 + ||(I-\Pi)p^h||_0 \\
&\leq ||(I-\Pi_1)\nabla \mathbf{u}||_0 + ||(I-\Pi_1)\nabla(\mathbf{u}-\mathbf{u}^h)||_0 + ||(I-\Pi)p||_0 + ||(I-\Pi)(p-p^h)||_0 \\
&\leq Ch||\nabla \mathbf{u}||_1 + C||\nabla(\mathbf{u}-\mathbf{u}^h)||_0 + Ch||p||_1 + C||p-p^h||_0 \\
&\leq C||\nabla(\mathbf{u}-\mathbf{u}^h)|| + C||p-p^h||_0.
\end{aligned}$$

This is (3.5).

To prove the global lower bound (3.6), we recall some standard approximation results. Let $\mathbf{v} \in \mathbf{H}^2(\Omega) \cap \mathbf{H}_0^1(\Omega)$, let $q \in L^2(\Omega)$, and denote by $I^h : \mathbf{V} \to \mathbf{V}^h$ the L^2-projection:

$$(\mathbf{v} - I^h\mathbf{v}, \mathbf{v}^h) = 0 \quad \forall \mathbf{v}^h \in \mathbf{V}^h. \tag{3.7}$$

We have (see [25])

$$||\mathbf{v} - I^h\mathbf{v}||_{0,T} \leq Ch||\mathbf{v}||_{1,T} \tag{3.8}$$

and

$$||\mathbf{v} - I^h\mathbf{v}||_{0,E} \leq Ch^{1/2}||\mathbf{v}||_{1,T}. \tag{3.9}$$

Subtracting (2.6) from (2.2) admits

$$\tilde{Q}(\mathbf{e}^h, \varepsilon^h; \mathbf{v}^h, q^h) + G(p, q^h) = 0 \quad \forall (\mathbf{v}^h, q^h) \in (\mathbf{V}^h, S^h).$$

Setting $(\mathbf{v}^h, q^h) = (I^h\mathbf{v}, 0)$ yields that

$$\tilde{Q}(\mathbf{e}^h, \varepsilon^h; I^h\mathbf{v}, 0) = 0.$$

Using integration by parts, using L^2 orthogonal projection (3.7), and observing that $\Delta\mathbf{u}^h$ vanishes on each element T, for arbitrary functions $\mathbf{f}^h \in \mathbf{V}^h$, we have

$$\begin{aligned}
&\tilde{Q}(\mathbf{e}^h, \varepsilon^h; \mathbf{v}, q) + G(\varepsilon^h, q) \\
&\quad = (\nabla\mathbf{e}^h, \nabla(\mathbf{v} - I^h\mathbf{v})) - (\varepsilon^h, \nabla\cdot(\mathbf{v} - I^h\mathbf{v})) - (q, \nabla\cdot\mathbf{e}^h) \\
&\quad = \sum_{T\in\tau_h} \left\{ (-\Delta\mathbf{e}^h + \nabla\varepsilon^h, \mathbf{v} - I^h\mathbf{v})_T + \frac{1}{2}\sum_{E\in\partial T\cap\Omega} \left(\left[\frac{\partial\mathbf{u}^h}{\partial\mathbf{n}}\right]_E, \mathbf{v} - I^h\mathbf{v} \right)_E \right\} + (q, \nabla\cdot\mathbf{u}^h) \\
&\quad = \sum_{T\in\tau_h} \left\{ (\mathbf{f} - \nabla p^h, \mathbf{v} - I^h\mathbf{v})_T + \frac{1}{2}\sum_{E\in\partial T\cap\Omega} \left(\left[\frac{\partial\mathbf{u}^h}{\partial\mathbf{n}}\right]_E, \mathbf{v} - I^h\mathbf{v} \right)_E \right\} + (q, \nabla\cdot\mathbf{u}^h) \\
&\quad = \sum_{T\in\tau_h} \left\{ (\mathbf{f} - \mathbf{f}^h - \nabla p^h, \mathbf{v} - I^h\mathbf{v})_T + \frac{1}{2}\sum_{E\in\partial T\cap\Omega} \left(\left[\frac{\partial\mathbf{u}^h}{\partial\mathbf{n}}\right]_E, \mathbf{v} - I^h\mathbf{v} \right)_E \right\} + (q, \nabla\cdot\mathbf{u}^h).
\end{aligned}$$

By applying inequalities (3.8) and (3.9), Lemma 3.1, and $||\nabla\cdot\mathbf{u}^h||_0 \le C||(I - \Pi)p^h||_0$, we obtain the following.

Case 1. If S^h is defined by (2.4), then

$$\begin{aligned}
&\tilde{Q}(\mathbf{e}^h, \varepsilon^h; \mathbf{v}, q) + G(\varepsilon^h, q) \\
&\quad \le \sum_{T\in\tau_h} \left\{ (||\mathbf{f} - \mathbf{f}^h||_{0,T} + ||\nabla p^h||_{0,T})||\mathbf{v} - I^h\mathbf{v}||_{0,T} \right. \\
&\qquad\qquad \left. + \frac{1}{2}\sum_{E\in\partial T\cap\Omega} \left\| \left[\frac{\partial\mathbf{u}^h}{\partial\mathbf{n}}\right]_E \right\|_{0,E} ||\mathbf{v} - I^h\mathbf{v}||_{0,E} \right\} \\
&\qquad + ||\nabla\cdot\mathbf{u}^h||_0||q||_0 \\
&\quad \le C\left\{ h||\mathbf{f} - \mathbf{f}^h||_{0,T} + h||\nabla p^h||_0 + h^{1/2}||[\nabla\mathbf{u}^h]||_{\Gamma_h} \right\} ||\mathbf{v}||_1 + C||(I - \Pi_0)p^h||_0||q||_0 \\
&\quad \le C\left\{ h||\mathbf{f} - \mathbf{f}^h||_0 + ||(I - \Pi_1)\nabla\mathbf{u}^h||_0 + ||(I - \Pi_0)p^h||_0 \right\} \{||\mathbf{v}||_1 + ||q||_0\} \\
&\quad \le C\left\{ h||\mathbf{f} - \mathbf{f}^h||_0 +^0 \eta_\Pi \right\} \{||\mathbf{v}||_1 + ||q||_0\}.
\end{aligned}$$

Case 2. If S^h is defined by (2.5) so that $\nabla p^h = 0$, then

$$\begin{aligned}
&\tilde{Q}(\mathbf{e}^h, \varepsilon^h; \mathbf{v}, q) + G(\varepsilon^h, q) \\
&\quad \le \sum_{T\in\tau_h} \left\{ ||\mathbf{f} - \mathbf{f}^h||_{0,T}||\mathbf{v} - I^h\mathbf{v}||_{0,T} + \frac{1}{2}\sum_{E\in\partial T\cap\Omega} \left\| \left[\frac{\partial\mathbf{u}^h}{\partial\mathbf{n}}\right]_E \right\|_{0,E} ||\mathbf{v} - I^h\mathbf{v}||_{0,E} \right\} \\
&\qquad + ||\nabla\cdot\mathbf{u}^h||_0||q||_0 \\
&\quad \le C\left\{ h||\mathbf{f} - \mathbf{f}^h||_{0,T} + h^{1/2}||[\nabla\mathbf{u}^h]||_{\Gamma_h} \right\} ||\mathbf{v}||_1 + C||(I - \Pi_1)p^h||_0||q||_0 \\
&\quad \le C\left\{ h||\mathbf{f} - \mathbf{f}^h||_0 + ||(I - \Pi_1)\nabla\mathbf{u}^h||_0 + ||(I - \Pi_1)p^h||_0 \right\} \{||\mathbf{v}||_1 + ||q||_0\} \\
&\quad \le C\left\{ h||\mathbf{f} - \mathbf{f}^h||_0 +^1 \eta_\Pi \right\} \{||\mathbf{v}||_1 + ||q||_0\}.
\end{aligned}$$

Because of $(\mathbf{e}^h, \varepsilon^h) \in (\mathbf{V}, S)$ and $Q(\mathbf{e}^h, \varepsilon^h; \mathbf{v}, q) = \tilde{Q}(\mathbf{e}^h, \varepsilon^h; \mathbf{v}, q) + G(\varepsilon^h, q)$, we get by (2.3) that

$$\begin{aligned}
|||(\mathbf{e}^h, \varepsilon^h)||| &\le \beta_1^{-1} \sup_{(\mathbf{v},q)\in(\mathbf{V},S)} \frac{Q(\mathbf{e}^h, \varepsilon^h; \mathbf{v}, q)}{||\mathbf{v}||_1 + ||q||_0} \\
&\le \beta_1^{-1} \sup_{(\mathbf{v},q)\in(\mathbf{V},S)} \frac{\tilde{Q}(\mathbf{e}^h, \varepsilon^h; \mathbf{v}, q) + G(\varepsilon^h, q)}{||\mathbf{v}||_1 + ||q||_0} \\
&\le C \left\{ \eta_\Pi + h||\mathbf{f} - \mathbf{f}^h||_0 \right\}.
\end{aligned}$$

Finally, the lower bound (3.6) holds. ∎

4. Implementation. The attractive feature of our error estimators is the great flexibility in the construction of the projection operator Π. The simplest way to accomplish this is to use a standard finite element projection or interpolation operator.

From a practical aspect, we expect that the choice of η_Π is simple and local, so the computation of Π or $I - \Pi$ should be done at the element level using only standard nodal data structures.

With the above discussion, a suitable choice of $I - \Pi_0$ based on two local quadrature rules is

$$||(I - \Pi_0)p^h||_{0,T} = \left\{ \int_{T,j \ (j\ge 2)} (p^h)^2 \mathbf{d}x - \int_{T,1} (p^h)^2 \mathbf{d}x \right\}^{1/2} \qquad \forall p^h \in S^h. \tag{4.1}$$

Here $\int_{T,k} g(x)\mathbf{d}x,\ k = 1, j$, denotes a quadrature formula as

$$\int_{T,k} g(x)\mathbf{d}x = \sum_{I=1}^{N(k)} g(x_I)\omega_I, \tag{4.2}$$

where x_I is the quadrature point, ω_I is the quadrature weight, and $N(k)$ is the number of quadrature points. By choosing a sufficient number of quadrature points at appropriate locations, along with suitable weights, we can construct quadrature rules of any order k. In particular, we can obtain a quadrature rule of order 1 with a single point, namely, the center of mass of the triangle.

Assume that $x_i,\ i = 1, 2, 3$, are the three vertices of element T. For linear polynomial $p^h \in S^h$, we obtain

$$\begin{aligned}
\int_{T,1} (p^h)^2 \mathbf{d}x &= |T| \left\{ p^h \left(\frac{x_1 + x_2 + x_3}{3} \right) \right\}^2 \\
&= |T| \left\{ \frac{p^h(x_1) + p^h(x_2) + p^h(x_3)}{3} \right\}^2 \\
&= \int_T (\Pi_0 p^h)^2 \mathbf{d}x \\
&= ||\Pi_0 p^h||^2_{0,T}.
\end{aligned}$$

Since $(p^h)^2$ is a quadratic polynomial, and thus $\int_{T,j} (p^h)^2 \mathbf{d}x,\ j \ge 2$, is exact for $\int_T (p^h)^2 \mathbf{d}x$, with $((I - \Pi_0)p^h, \Pi_0 p^h) = 0$, we can derive

$$||(I - \Pi_0)p^h||^2_{0,T} = ||p^h||^2_{0,T} - ||\Pi_0 p^h||^2_{0,T} = \int_{T,j} (p^h)^2 \mathbf{d}x - \int_{T,1} (p^h)^2 \mathbf{d}x. \tag{4.3}$$

Then, we obtain (4.1) easily.

Remark 5. It is easy to see that $I - \Pi_0$ can be computed at the element level. Moreover, we can prove $((I - \Pi_0)p^h, \Pi_0 p^h) = 0$ as follows. Since $p^h \in S^h$ is a linear polynomial, $\int_{T,1} p^h \mathbf{d}x$ is exact for $\int_T p^h \mathbf{d}x$, and therefore,

$$\begin{aligned}
||\Pi_0 p^h||_{0,T}^2 &= \int_{T,1} (p^h)^2 \mathbf{d}x \\
&= |T| \left\{ p^h \left(\frac{x_1 + x_2 + x_3}{3} \right) \right\}^2 \\
&= \left\{ p^h \left(\frac{x_1 + x_2 + x_3}{3} \right) \right\} * \int_{T,1} p^h \mathbf{d}x \\
&= \left\{ p^h \left(\frac{x_1 + x_2 + x_3}{3} \right) \right\} * \int_{T} p^h \mathbf{d}x \\
&= \int_T p^h * \Pi_0 p^h \mathbf{d}x \\
&= (p^h, \Pi_0 p^h).
\end{aligned}$$

Thus, $((I - \Pi_0)p^h, \Pi_0 p^h) = 0$.

A suitable choice of Π_1 is to define its interpolation by using a projection onto the dual volume associated with each node. To be more precise, let τ denote a given triangulation of the domain Ω. For each node x^k, $k = 1, 2, \ldots, N$, let $S^k \subset \Omega$ denote the union of triangles that share the common vertex x^k. For each k, define by ϕ^k the continuous, piecewise linear basis function such that $\phi^k(x^m) = \delta_{k,m}$. Then $S^k = \mathtt{supp}\{\phi^k\}$.

Since $\nabla \mathbf{u}^h$ and p^h are the piecewise constant velocity deformation tensor and piecewise constant pressure, respectively, there is no technical difference in constructing Π_1 for $\nabla \mathbf{u}^h$ and p^h. For simplicity, we give the details of only the construction of $\Pi_1 p^h$.

Given a function $q \in L^2(\Omega)$, let q^k be a constant function on S^k, which minimizes the functional

$$J_k(q^k) = \frac{1}{2} \int_{S^k} (q - q^k) d\Omega. \tag{4.4}$$

Then, we define

$$\Pi_1 q = \sum_{k=1}^{N} q^k \phi^k \in S_h. \tag{4.5}$$

When choosing $q = p^h \in R_0$, we can simplify the functional (4.4) as

$$J_k(q^k) = \sum_{T \in S^k} V^k(T)(p_T - q^k)^2, \tag{4.6}$$

where p_T is the restrict of p^h on element T and $V^k(T)$ is the volume of the element $T \in S^k$. Minimization of J_k yields the formula

$$q^k = \frac{\sum_{T \in S^k} V^k(T) p_T}{\sum_{T \in S^k} V^k(T)}. \tag{4.7}$$

Obviously, the nodal values of $\Pi_1 p^h$ are area-weighted averages of the surrounding constant pressure p^h.

Now, the local gradient projection error estimator can be obtained by (4.7) as follows:

$$||(I-\Pi_1)p^h||_{0,T} = ||p^h - \sum_{x^k \in T} q^k \phi^k||_{0,T}. \tag{4.8}$$

The choice of $\Pi_1 \nabla \mathbf{u}^h$ is the same as $\Pi_1 p^h$. At first, we derive the formula of the constant velocity deformation tensor $\mathbf{v}^k$:

$$\mathbf{v}^k = \frac{\sum_{T \in S^k} V^k(T) \nabla \mathbf{u}_T}{\sum_{T \in S^k} V^k(T)}. \tag{4.9}$$

Then, we obtain the local gradient projection error estimator

$$||(I-\Pi_1)\nabla \mathbf{u}^h||_{0,T} = ||\nabla \mathbf{u}^h - \sum_{x^k \in T} \mathbf{v}^k \phi^k||_{0,T}. \tag{4.10}$$

Obviously, from the definition of Π_1 in (4.5), the assumptions of (2.12) and (2.13) are valid. In the following, we will show that Π_1 can be computed locally at the element level, and $\Pi_1 p_h$ and $\Pi_1 \nabla u_h$ are continuous over each element.

To show that Π_1 is computed locally, we introduce one layer of oversampling over element T defined by

$$O_T = \sum_{x^k \in T} S^k, \tag{4.11}$$

as shown in Figure 4.1.

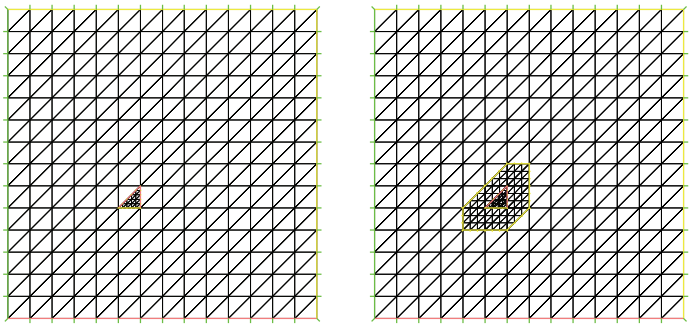

FIG. 4.1. *Left: element T. Right: one layer of oversampling O_T.*

Since the information including $V^k(T)$, p_T, and $\nabla \mathbf{u}_T$ for computing q^k and $\mathbf{v}^k$ can be obtained in O_T for $x^k \in T$, Π_1 can be computed locally at the element level with one layer of oversampling. Moreover, $\Pi_1 p_h$ and $\Pi \nabla u_h$ are continuous across the element boundary. Additionally, since local error estimators are independent of each other, they can be carried out in parallel perfectly, as can q^k and $\mathbf{v}^k$.

Remark 6. The two local quadrature rules were first developed to circumvent the inf-sup condition in [22]; later, they were used to improve variational multiscale methods in [27]. The construction of Π_1 was first used to stabilize the lowest order conforming pair ($\mathbf{P}1-P0$) in [21]. However, in their work, either Π_0 or Π_1 is designed

implicitly and mainly acts on the pressure as a stabilization norm. On the contrary, in our work, we define the projection error estimators by constructing Π_0 and Π_1 explicitly, which will be easier to computed locally.

5. Numerical tests. To illustrate our theoretical results, we consider three related numerical tests in this section. The first is a smooth problem, while the second is a singular problem, and the third deals with a benchmark problem. The experiments are all implemented in the two-dimensional framework using public domain finite element software FreeFem++ [28].

The adaptive strategy for computation is carried out as follows.

First, set a tolerance η^*; then we start from an initial triangulation τ_0 and compute η_Π.

• Step 1: If $\eta_\Pi \leq \eta^*$, stop. We obtain the final finite element solution. Otherwise, go to Step 2.

• Step 2: Compute $\eta_{\Pi,T}$ and η_Π, generate a new mesh size h by the strategy presented in [28], and recompute η_Π based on this new triangulation. Then go back to Step 1.

Commonly, the circle of Steps 1 and 2 is iterated N times, where N equals 3 or 4.

For convenience of presentation, we introduce the following notation:

• Dof := number of elements for triangulation τ_j;

• $Eff_\eta := \eta^j/e_j$, effective index, i.e., the ratio between the related estimator and the true error. Here $e_j =: |||(\mathbf{e}^j, \varepsilon^j)|||$ and η can be either ${}^0\eta_\Pi$ or ${}^1\eta_\Pi$;

• r_e=$|||(\mathbf{e}, \varepsilon)|||/|||(\mathbf{u}, p)|||$ denotes the relative error with respect to the sum of the velocity in the H^1-norm and the pressure in the L^2-norm.

In the following, we first solve the two stabilized mixed low-order finite element methods for the Stokes problem on a coarse triangulation. Then, we refine the mesh either uniformly or adaptively based on the estimator η_Π according to (3.1). Next, We discuss the efficiency of our methods based on the following two cases:

Case 1. Using a stabilized $\mathbf{P}1 - P1$ pair based on estimator ${}^0\eta_\Pi$.

Case 2. Using a stabilized $\mathbf{P}1 - P0$ pair based on estimator ${}^1\eta_\Pi$.

5.1. A smooth problem. The first example is the following flow problem with a smooth solution:

$$\begin{aligned} u_1 &= 2\pi \sin^2(\pi x)\sin(\pi y)\cos(\pi y), \\ u_2 &= -2\pi \sin(\pi x)\cos(\pi x)\sin^2(\pi y), \\ p &= \cos(\pi x)\cos(\pi y), \end{aligned}$$

where domain $\Omega = [0,1] \times [0,1]$ with zero Dirichlet boundary condition.

For uniform refinements, the successive meshes are obtained by decomposing the unit square into $N \times N$ equal squares and then dividing every square into two triangles. This is done for $N = 10, 15, 20, 25$. The mesh for $N = 10$ is shown in the left side of Figure 5.1.

For adaptive refinements, we start with an initial mesh generated with the Delaunay triangulation at $h = 0.1$, which is shown in the right side of Figure 5.1.

Results for the two stabilized methods based on related estimators are given in Tables 5.1–5.4. From those tables, we note that both uniform refinements and adaptive refinements get good approximate solutions as $h \to 0$, and the convergence orders are nearly optimal (about 1.0). However, to obtain similar accuracy, the adaptive refinements will use less meshes. In addition, for either uniform refinements or adaptive

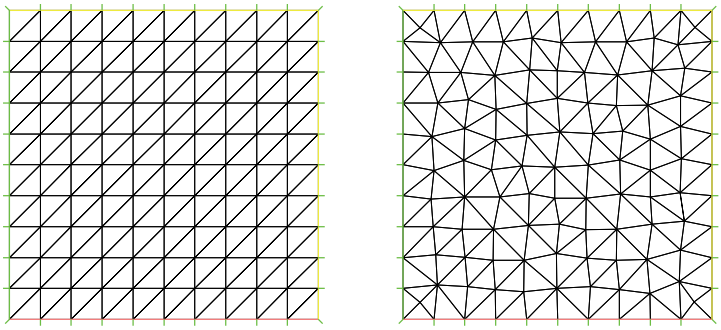

FIG. 5.1. *Initial triangulations. Left: uniform. Right: adaptive.*

TABLE 5.1
Case 1. *Effectivity indices for stabilized* $\mathbf{P}1 - P1$ *pair for uniform refinements.*

Level	Dof	r_e	Order	$Eff_{0_{\eta_\Pi}}$
0	200	0.2590	-	1.0207
1	450	0.1724	1.0038	1.0181
2	800	0.1291	1.0061	1.0131
3	1250	0.1031	1.0056	1.0097

TABLE 5.2
Case 1. *Effectivity indices for stabilized* $\mathbf{P}1 - P1$ *pair for adaptive refinements.*

Level	Dof	r_e	Order	$Eff_{0_{\eta_\Pi}}$
0	208	0.2394	-	1.0270
1	334	0.1861	1.0625	1.0168
2	577	0.1343	1.1935	1.0291
3	1040	0.0956	1.1541	1.0197

TABLE 5.3
Case 2. *Effectivity indices for stabilized* $\mathbf{P}1 - P0$ *pair for uniform refinements.*

Level	Dof	r_e	Order	$Eff_{1_{\eta_\Pi}}$
0	200	0.3048	-	0.9619
1	450	0.2033	0.9991	0.9837
2	800	0.1521	1.0086	0.9909
3	1250	0.1214	1.0091	0.9941

TABLE 5.4
Case 2. *Effectivity indices for stabilized* $\mathbf{P}1 - P0$ *pair for adaptive refinements.*

Level	Dof	r_e	Order	$Eff_{1_{\eta_\Pi}}$
0	208	0.2719	-	0.9885
1	320	0.2093	1.2151	0.9946
2	528	0.1557	1.1800	1.0165
3	940	0.1158	1.0267	1.0018

refinements, since the effective indices $Eff_{0_{\eta_\Pi}}$ and $Eff_{1_{\eta_\Pi}}$ approach 1.0, both projection estimators ${}^0\eta_\Pi$ and ${}^1\eta_\Pi$ stay very close to the true error. In fact, the error estimators are almost exact.

5.2. A singular problem. In the second example, we consider Ω as a disk of radius 1 with a crack joining the center to the boundary as presented in [14], and the exact solution with the velocity $\mathbf{u} = (u_1, u_2)$ and pressure p is given as follows:

$$u_1 = 1.5r^{1/2}(\cos(0.5\theta) - \cos(1.5\theta)),$$
$$u_2 = 1.5r^{1/2}(3\sin(0.5\theta) - \sin(1.5\theta)),$$
$$p = -6/r^{1/2}\cos(0.5\theta),$$

where (r, θ) is a polar representation of a point in the disk and is singular at the end of the crack, i.e., at the center of the disk. $\mathbf{f}$ is determined by (2.1) and $\mathbf{u}$ is enforced with appropriate inhomogeneous boundary conditions.

This test begins with the same initial triangulation for both cases. As shown in Figure 5.2, the left side of the figure is the initial mesh, while the right is the final uniform refinement. The final adaptive refinements for the two stabilized methods are shown in Figure 5.3. Based on Tables 5.5 and 5.6 and Figures 5.2 and 5.3, the observations and conclusions of this experiment are presented as follows.

• For both cases, our stabilized methods on adaptive refinements obtain much better approximation solutions than the uniform refinements; meanwhile, adaptive refinements require fewer meshes than uniform refinements. See Table 5.5.

• From Table 5.5, we find that, at the final refinement, all effective indices do not approach 1.0. However, those effective indices of adaptive refinements are much better for approaching 1.0 than in the uniform case. In addition, in Table 5.6 the effective indices of adaptive refinements at each level increase to approach 1.0, which implies that the projection error estimators approximate to the true error asymptotically in both cases.

• Note that, for both cases, after some successive iterations the convergence orders of uniform refinements are only 0.4–0.5, while the convergence rates of adaptive refinements are a little over the optimal order 1. These results imply that adaptive refinements are much more efficient than uniform refinements for the singular problem.

• Figure 5.3 shows that, for both cases, after some successive iterations local mesh refinements are applied near the crack due to the crack singularity and produce very similar refinements. However, the right side of Figure 5.2 shows that uniform refinement refines the entire area and requires much unnecessary work.

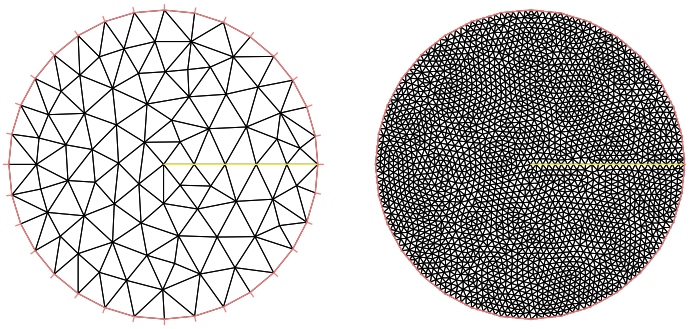

FIG. 5.2. *Left: initial triangulation for both methods. Right: uniform refinement for both stabilized methods.*

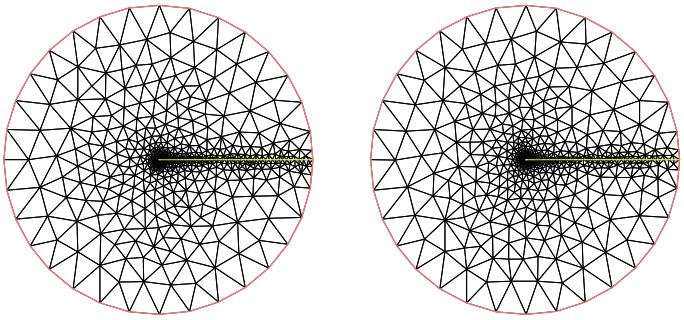

FIG. 5.3. *Adaptive refinements for stabilized methods. Left: stabilized* $\mathbf{P}1 - P1$ *pair based on* ${}^0\eta_\Pi$. *Right: stabilized* $\mathbf{P}1 - P0$ *pair based on* ${}^1\eta_\Pi$.

TABLE 5.5
Comparison of uniform refinement and local refinement strategies.

Type	Strategy	Dof	r_e	Order	Eff_{η_Π}
Case 1	Uniform	4670	0.2303	0.4896	0.5440
	Adaptive	1251	0.1078	1.5556	0.8027
Case 2	Uniform	4670	0.2068	0.5202	0.6039
	Adaptive	1202	0.0976	1.5940	0.8944

TABLE 5.6
The effective indices of the projection error estimators and adaptive refinements, respectively.

	Level	0	1	2	3	4
Case 1	$Eff_{{}^0\eta_\Pi}$	0.5105	0.6017	0.7090	0.7692	0.8027
Case 2	$Eff_{{}^1\eta_\Pi}$	0.5099	0.5958	0.7582	0.8228	0.8944

5.3. Lid driven cavity. The last example is the "lid driven cavity," which is a popular benchmark problem for testing numerical schemes. In this test, fluid is enclosed in a square box, with an imposed velocity of unity in the horizontal direction on the top boundary, and a no slip condition on the remaining walls. As we know, there are two singularities arising at the top corners of the square box.

First, we start with an initial mesh for both cases generated from the Delaunay triangulation with $h = 0.1$; see the left parts of Figures 5.4 and 5.5.

From Figures 5.4 and 5.5, we note that, for both cases, in the successive iterations the adaptive strategies create more triangles in the two upper corners of the cavity due to the two singularities. It can also be seen that the pattern of refinement away from the singularity differs depending on the error estimator used, which confirms our expectation. In addition, the meshes generated by both stabilized methods based on the related error estimators are very similar.

Finally, in order to show the prominent features of our adaptive stabilized methods, in Figure 5.6 we draw the pressure level lines for the driven cavity for both stabilized methods at the final refinements. The figure shows that both adaptive stabilized methods are stable without oscillations, and since the singular nature of the pressure is well captured in the final adaptive meshes, the methods also improve the quality of the approximate solutions.

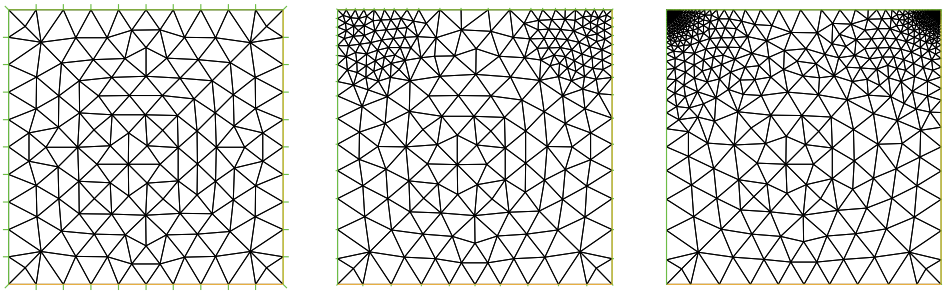

FIG. 5.4. *Adaptive refinement for the stabilized* $\mathbf{P}1 - P1$ *pair based on* ${}^0\eta_\Pi$. *From left to right: initial triangulation* τ_0, *first refinement, final refinement.*

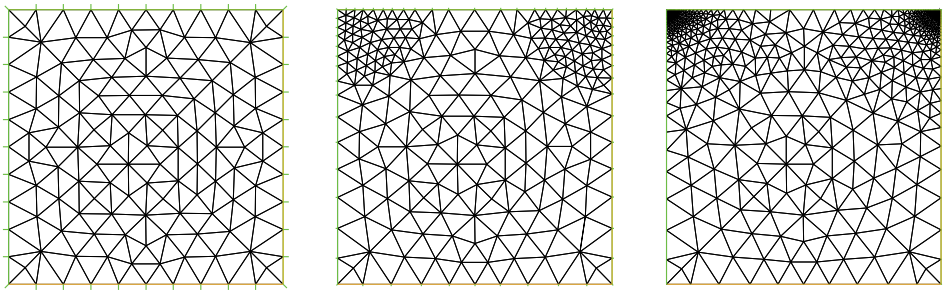

FIG. 5.5. *Adaptive refinement for the stabilized* $\mathbf{P}1 - P0$ *pair based on* ${}^1\eta_\Pi$. *From left to right: initial triangulation* τ_0, *first refinement, final refinement.*

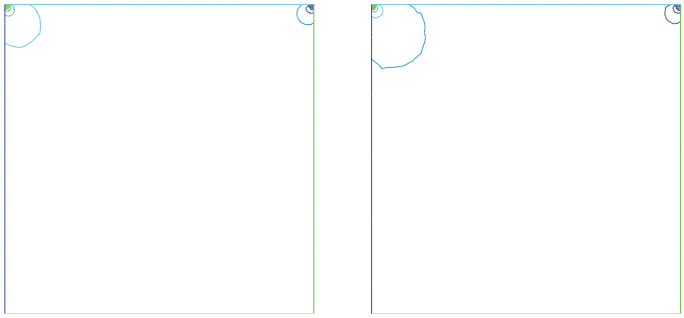

FIG. 5.6. *The pressure level lines for the driven cavity at the final refinements. Left: the stabilized* $\mathbf{P}1 - P1$ *pair based on* ${}^0\eta_\Pi$. *Right: the stabilized* $\mathbf{P}1 - P0$ *pair based on* ${}^1\eta_\Pi$.

6. Conclusions. In this paper, we have derived an efficient and effective adaptive strategy for the stabilization of mixed low-order finite elements for the Stokes problem based on two projection error estimators. Global upper and lower bounds are proved, and the tests show that both projection error estimators are easy to compute. Our main conclusion is that the projection error estimators provide an effective way to estimate the local discretization error of some flow problems.

Acknowledgments. The authors thank the referees and editors for their valuable comments and suggestions which helped to greatly improve the paper.

REFERENCES

[1] I. Babuška and W. C. Rheinboldt, *A posteriori error estimates for the finite element method*, Internat. J. Numer. Methods Engrg., 12 (1978), pp. 1597–1615.

[2] I. Babuška and W. C. Rheinboldt, *Error estimates for adaptive finite element computations*, SIAM J. Numer. Anal., 15 (1978), pp. 736–754.

[3] R. Verfurth, *A Review of A Posteriori Error Estimation and Adaptive Mesh-Refinement Techniques*, Wiley/Teubner, Stuttgart, 1996.

[4] C. Carstensen and R. Verfürth, *Edge residuals dominate a posteriori error estimates for low order finite element methods*, SIAM J. Numer. Anal., 36 (1999), pp. 1571–1587.

[5] M. Ainsworth and J. T. Oden, *A Posteriori Error Estimation in Finite Element Analysis*, Wiley-Interscience, New York, 2000.

[6] R. E. Bank and R. K. Smith, *A posteriori error estimates based on hierarchical bases*, SIAM J. Numer. Anal., 30 (1993), pp. 921–935.

[7] R. E. Bank, *Hierarchical bases and the finite element method*, Acta Numer., 5 (1996), pp. 1–43.

[8] R. E. Bank and A. Weiser, *Some a posteriori error estimators for elliptic partial differential equations*, Math. Comp., 44 (1985), pp. 283–301.

[9] O. C. Zienkiewicz and J. Zhu, *A simple error estimator and adaptive procedure for practical engineering analysis*, Internat. J. Numer. Methods Engrg., 24 (1987), pp. 337–357.

[10] O. C. Zienkiewicz and J. Zhu, *The superconvergence patch recovery and a posteriori error estimates, part* I: *The recovery technique*, Internat. J. Numer. Methods Engrg., 33 (1992), pp. 1331–1364.

[11] O. C. Zienkiewicz and J. Zhu, *The superconvergence patch recovery and a posteriori error estimates, part* II: *Error estimates and adaptivity*, Internat. J. Numer. Methods Engrg., 33 (1992), pp. 1365–1382.

[12] R. E. Bank and J. Xu, *Asymptotically exact a posteriori error estimators, part* I: *Grids with superconvergence*, SIAM J. Numer. Anal., 41 (2003), pp. 2294–2312.

[13] A. Naga and Z. Zhang, *A posteriori error estimates based on the polynomial preserving recovery*, SIAM J. Numer. Anal., 42 (2004), pp. 1780–1800.

[14] R. Verfurth, *A posteriori error estimators for the Stokes equations*, Numer. Math., 55 (1989), pp. 309–325.

[15] R. E. Bank and B. D. Welfert, *A posteriori error estimates for the Stokes problem*, SIAM J. Numer. Anal., 28 (1991), pp. 591–623.

[16] M. Ainsworth and J. T. Oden, *A posteriori error estimators for the Stokes and Oseen equations*, SIAM J. Numer. Anal., 34 (1997), pp. 228–245.

[17] D. Kay and D. Silvester, *A posteriori error estimation for stabilized mixed approximations of the Stokes equations*, SIAM J. Sci. Comput., 21 (1999), pp. 1321–1336.

[18] F. Brezzi and M. Fortin, *Mixed and Hybrid Finite Element Methods*, Springer-Verlag, Berlin, New York, 1991.

[19] D. N. Arnold, F. Brezzi, and M. Fortin, *A stable finite element for the Stokes equations*, Calcolo, 23 (1984), pp. 337–344.

[20] C. Dohrmann and P. Bochev, *A stabilized finite element method for the Stokes problem based on polynomial pressure projections*, Int. J. Numer. Methods Fluids, 46 (2004), pp. 183–201.

[21] P. B. Bochev, C. R. Dohrmann, and M. D. Gunzburger, *Stabilization of low-order mixed finite elements for the Stokes equations*, SIAM J. Numer. Anal., 44 (2006), pp. 82–101.

[22] J. Li and Y. N. He, *A stabilized finite element method based on two local Gauss integrations for the Stokes equations*, J. Comput. Appl. Math., 214 (2008), pp. 58–65.

[23] V. Girault and P.-A. Raviart, *Finite Element Methods for the Navier-Stokes Equations: Theory and Algorithms*, Springer Ser. Comput. Math. 5, Springer, Berlin, 1986.

[24] M. Gunzburger, *Finite Element Methods for Viscous Incompressible Flows: A Guide to Theory, Practice and Algorithms*, Academic Press, Boston, 1989.

[25] P. G. Ciarlet, *The Finite Element Method for Elliptic Problems*, Classics in Appl. Math. 40, SIAM, Philadelphia, 2002.

[26] W. Dorfler and R. H. Nochetto, *Small data oscillation implies the saturation assumption*, Numer. Math., 91 (2002), pp. 1–12.

[27] H. B. Zheng, Y. R. Hou, F. shi, and L. N. Song, *A finite element variational multiscale method for incompressible flows based on two local Gauss integrations*, J. Comput. Phys., 228 (2009), pp. 5961–5977.

[28] FreeFem++, *Version* 2.17.1, http://www.freefem.org/ff++/ftp/ (2008).